Study of Fracture Parameter Using COMSOL-multiphysics For Curved Cracked Bimodular Flexural Specimen

Awani Bhushan*[1], S.K. Panda[1].
[1]Indian Institute of Technology (BHU) Varanasi
*Corresponding author: Department of Mechanical Engineering, IIT (BHU) Varanasi, awanibhu@gmail.com, abhushan.rs.mec13@itbhu.ac.in

Abstract: The computation of *J*-integral for curve geometry is a challenging task even for a unimodular case due to the presence of additional area integral term due to its geometrical correction factor. The formulation of bimodular stress field is based on stress dependent elasticity and the simulations have been carried out using commercial finite element software COMSOL Multiphysics 4.4. The complexity of the problem is enhanced due to adding bimodular stress field in the evaluation of complex *J*-integral ($\hat{J}_F$) for curve cracked geometry subjected to standard three point loading conditions. It has been observed from the simulations that complex J-integral is almost independent of its path. The analysis of stress distribution and measurement of neutral axis shift has been done due to bimodularity. The severity of bimodular 2D curved crack progression behavior has been delineated with asymmetry of stress-distribution and distortion of neutral axis.

Keywords: Curved crack**,** *J*-integral, bi-modular material, nuclear grade graphite, stress dependent elasticity,

1. Introduction

St. Venant recognized that certain actual materials have different elastic behavior when they are loaded in tension as compared to compression in 1826 [1]. Though, the concept of such materials which are showing different moduli in tension and compression was not devised by Timoshenko as bimodular materials in pure bending [2]. For the beam subjected to pure bending condition, Marin derived the expression for effective stiffness for such materials [3]. The bimodulus concept was extended to two-dimensional materials by Ambartsumyan [4-6]. Within the last few decades, several attempts have been made to establish constitutive relationships for such materials and develop analytical and numerical solutions for the bending and shear deformation of bimodular beams [7-14].

Due to their stability at higher temperature, high-temperature strength, lighter weight, better erosion, corrosion and oxidation resistance, lower thermal conductivity, lower cost, and wider availability; advance ceramic used in various applications and most of them are showing bimodularity. In flexural condition, ceramics fails due to tensile flexural strength cross the critical limit. The lack of ductility and yielding capability offers ceramic materials their most undesirable characteristics such as low strain tolerance, low fracture toughness [15]. Failures in such brittle materials with very low strength may take place due to pre-existing flaws/defects or crack and its subsequent growth into defect-free regions with disastrous consequences to human life, often involving large-scale financial loss. Therefore it is essential to characterize quantitative the residual strength of material in the presence of cracks/ defects. The energy concepts of correlation with crack extension based on fracture mechanics has been very useful in the accurate failure prediction [16]. Eshelby, Cherepanov and Rice played a very significant role in the advancement of static fracture mechanics [17-19]. Rice's J-integral comprises the salient features like it has the physical interpretation of equivalent energy release rate (G); it has the property of path independence and it can be related to the stress intensity factors. Within few decades a lot of effort has been done on the extensions of J-integral for different geometry and loading condition by the several researchers which includes analytical derivation as well computational estimation but focused on only straight or arbitrarily kinked crack geometry [20-25].

In contrast, it is very well-known that the crack geometry is one of the major parameters that affect the overall resistance against fracture for many structures. Due to complex design and their applicability of non-uniform load may lead

to appearance of curved cracks more expected than that of straight cracks. The curved cracks are also originated frequently in bimaterial interfaces. Some researchers have been worked on the curved crack geometry with various loading configuration to characterizing crack parameters like stress intensity factor, J-integral [26-33]. The strength of advance ceramics is affected by bimodular behaviour of material and also affected the cracked parameter in straight crack geometry is studied by [34-36].

This paper deals with the effect of bimodularity on crack characterizing parameter specifically complex path independent integral ($\hat{J}_f$) derived by [28] from the appropriate energy balance expression has been proposed for a two-dimensional stationary circular arc crack subjected to various loads. In contrast, this paper is limited to static loading within linear elastic fracture mechanics (LEFM) region, because ceramic have lack of ductility and yielding.

2. Finite Element Model

2.1 Specimen Geometry

A semi-circular crack geometry is emanating from the mid line of the lower surface and subjected to the three point flexural loading as shown in Figure 1.

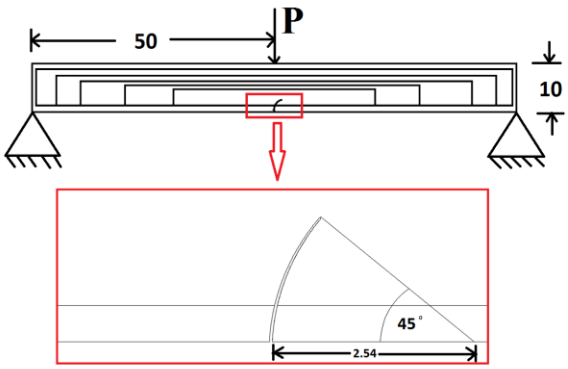

Figure 1: Circular arc cracked flexural specimen with five contours for which complex J-integral value evaluated and the arc length is 2 mm radius 2.54mm.

The length of an edge curve crack is 2 mm whereas the radius is 2.54 mm (1inch). The crack made 45^0 angle from the bottom surface. The two faces of the crack are radially parallel and the distance between the two faces is .02 mm. The length of specimen is 100 mm and the height of the specimen is 10 mm. The applied load P is quantitatively equal to 500 N. The two dimensional finite element simulations were performed for nuclear grade graphite (grade 2020) and its mechanical properties were taken from Graphite design handbook [37]. The Young's Modulus of elasticity for this graphite in tensile loading is found to be 7.14 GPa whereas in compressive loading is 3.89 GPa as overall E_T/E_C ratio is 1.83 .

2.2 Finite Element Model

The two dimensional model has been prepared using finite element software package COMSOL Multiphysics 4.4 [38]. After the mesh convergent study, the final mesh model has been made-up of overall 3090 elements, in which 3015 quadratic elements and 75 triangular elements as shown in Figure 2.

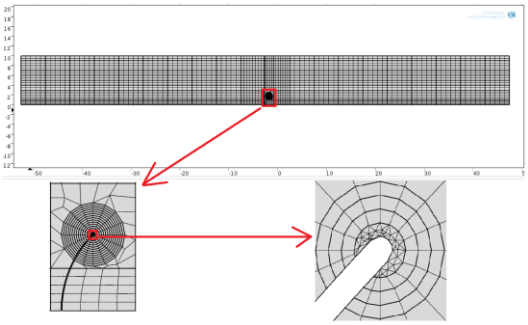

Figure 2: Finite Element mesh for geometrical curve cracked model

2.3 Mathematical formulation for Bimodularity

Some natural and artificial materials which exhibit different elastic moduli in compression and tension are called as bimodular materials. In the flexural testing, when subjected to three point loading condition, the effect of bimodularity really works on the basis of stress dependent elasticity, because the top half portion of the specimen possess compressive stress region and

the other half of the portion possess tensile stress region. The implementation of this property in finite element model is quite challenging task. The model formulation has been done using stress dependent elasticity, and the following steps are availing the bi-modular formulation:

1. 1st iteration is the linear model formation where taking some arbitrary value of Young's Modulus of elasticity. That means the model is solved for unimodular condition, then after we found the stress distribution at each node.

2. Sense the stress value at each node.

3. Evaluate the value of variable p at each node. where p is negative hydrostatic stress.

$$p = -\left(\frac{\sigma_{xx} + \sigma_{yy} + \sigma_{zz}}{3}\right) \quad (1)$$

4. For next iteration we have to put the E_T (Young's Modulus of elasticity in tension) and E_C (Young's Modulus of elasticity in compression) according to following criteria, where Young's Modulus of elasticity is defined by a step function.

5. The modulus of elasticity of material is define a step function, which sense the value of p

$$E(p) = \begin{Bmatrix} E_T where, -p \\ E_C where, +p \end{Bmatrix} \quad (2)$$

6. Putting the E_T and E_C value at the nodes by finding where the value is -p and +p respectively and again solve the problem.

7. The iteration continues until the error became less than tolerance limit.

8. So, the duration of solving the problem is greatly increased by mesh refinement and reducing the tolerance limit.

9. So, finding appropriate solution in 3D is quite a difficult task because the solution time is too long.

3. Path independent integral $\hat{J}_F$

In the present study, the investigation of the performance of integral $\hat{J}_F$ under the applied bimodular stress field for nuclear grade graphite (grade 2020) [37] for an edge circular cracked beam undergoing flexural loading deformation, as shown in Figure 3. The curved crack borders are assumed traction-free. Recalling the path independent integral expression $\hat{J}_F$ [28], the energy release rate is given by

$$\hat{J}_F = \int_{\Gamma_A} (W\hat{n}_\beta - \hat{T}_i \hat{u}_{i;\beta}) d\Gamma - \int_A \frac{1}{r} \hat{\sigma}_{i\beta} \hat{u}_{i;r} dA + [\int_A \hat{\sigma}_{ij} \hat{\varepsilon}^{th}_{ij;\beta} dA + \int_A \hat{\sigma}_{ij} \hat{\varepsilon}^{o}_{ij;\beta} dA + \int_A \rho \hat{\ddot{u}}_i \hat{u}_{i;\beta} dA - \int_A \hat{B}_i \hat{u}_{i;\beta} dA] \quad (3)$$

where,

β, Ψ Angle

W Strain energy density

n_β Unit outward positive normal vector on $d\Gamma$ in β direction.

$\sigma^{i\beta}$ Stress tensors

σ^{ij} Stress tensors

ε^{th}_{ij} Thermal Strain Tensor

ε^{o}_{ij} Initial Strain Tensor

Γ_A Arbitrary Curve surrounding A

B^i Body force vector

u_i Displacement vector

$\ddot{u}^i$ Material acceleration vector

ρ Density

ε_{ij} Strain tensor

$\hat{n}_\beta$ Physical components of the tensor n_β

T^i Traction Vector

$\hat{T}_i$ Physical components of the tensor T^i

$\hat{\sigma}_{i\beta}$ Physical components of the tensor $\sigma^{i\beta}$

$\hat{\sigma}_{ij}$ Physical components of the tensor σ^{ij}

$\hat{\ddot{u}}_i$ Physical components of the tensor $\ddot{u}^i$

$\hat{B}_i$ Physical components of the tensor B^i

$\hat{u}_{i;\beta}$ Physical components of the covariant derivative $u_{i,r}$

$\hat{u}_{i;r}$ Physical components of the covariant derivative $u_{i,\beta}$

$\hat{\varepsilon}^{th}_{ij;\beta}$ Physical components of the covariant derivative $\varepsilon^{th}_{ij,\beta}$

$\hat{\varepsilon}^{o}_{ij;\beta}$ Physical components of the covariant derivative $\varepsilon^{o}_{ij,\beta}$

The subscript resembles to the covariant and superscript, contra-variant tensor properties. The first two integrals in the right hand side of the above expression (3) is equivalent to the *F*-integral for circular arc crack [27]. For infinite crack radius the area integral vanishes and the expression leading to the illustrious Rice's *J*-integral [19]. The area integral expressions within the square brackets in Eq. (3) represent the correction terms to preserve path independence of $\hat{J}_F$ integral due to thermal strain, initial strain, material inertia and body force effects in respective progression.

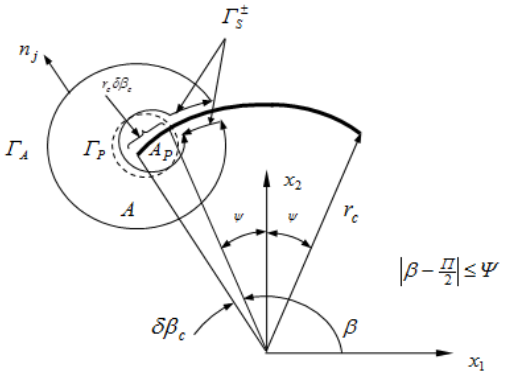

Figure 3: Configuration of a crack tip; A_P Fracture process region, Γ_P Boundary of A_P, Γ_A Arbitrary curve surrounding *A*, $\Gamma_S^{\pm}$ Curves along the traction-free crack surfaces.

For the numerical estimation of path independence under bimodular stress field (only), the other integrals in the expression (3) due to inertia, thermal or initial strain and body force effects are neglected, the $\hat{J}_F$ turns into

$$\hat{J}_F = \int_{\Gamma_A} (W\hat{n}_\beta - \hat{T}_i\hat{u}_{i;\beta})d\Gamma - \int_A \left(\frac{1}{r}\hat{\sigma}_{i\beta}\hat{u}_{i;r}\right)dA \tag{4}$$

The expression for $\hat{J}_F$ has been developed in polar coordinate system. Generally, the finite element commercial packages provide output data in the Cartesian system, which can directly be used in the estimation of $\hat{J}_F$ when this integral is expressed in global Cartesian form. The details of transformations are available in [29].

The line integral in Eq. (4) on transformation to Cartesian coordinates becomes

$$\int_{\Gamma_A} (W\hat{n}_\beta - \hat{T}_i\hat{u}_{i;\beta})d\Gamma \Leftrightarrow$$

$$\int_{\Gamma_A} [-W\cos\beta - \{\sigma^{xy}(\frac{\partial u_x}{\partial x}\sin\beta - \frac{\partial u_x}{\partial y}\cos\beta) + \sigma^{yy}(\frac{\partial u_y}{\partial x}\sin\beta - \frac{\partial u_y}{\partial y}\cos\beta)\}]dx -$$

$$\int_{\Gamma_A} [W\sin\beta + \{\sigma^{xx}(\frac{\partial u_x}{\partial y}\cos\beta - \frac{\partial u_x}{\partial x}\sin\beta) - \sigma^{xy}(\frac{\partial u_y}{\partial x}\sin\beta - \frac{\partial u_y}{\partial y}\cos\beta)\}]dy \tag{5}$$

The area integral in Eq. (4) becomes

$$\int_A \frac{1}{r}\hat{\sigma}_{i\beta}\hat{u}_{i;r}dA \Leftrightarrow$$

$$\int_A \frac{1}{r}\left[(\sigma^{xy}\cos\beta - \sigma^{xx}\sin\beta)\left(\frac{\partial u_x}{\partial x}\cos\beta + \frac{\partial u_y}{\partial y}\sin\beta\right) + (\sigma^{yy}\cos\beta - \sigma^{xy}\sin\beta)\left(\frac{\partial u_y}{\partial x}\cos\beta + \frac{\partial u_y}{\partial y}\sin\beta\right)\right]dA \tag{6}$$

3.1 Computation of Complex *J*-integral $\hat{J}_F$

The estimation of complex *J*-integral $\hat{J}_F$ for 5 contours is used as shown in the Figure 1. The line integral is evaluated for the following contours (shown in Figure 1) whereas area integral is evaluated for the area enclosed by the same contour. The complex *J*-integral $\hat{J}_F$ is transformed from polar coordinate system to Cartesian coordinate system as equation (5) and (6) and values are estimated by post-processing.

4. Results and Discussion

The figure 4 and 5 represents the stress distribution in x-direction in the whole geometry as well as around the crack tip. Stress concentration near the crack tip is clearly visible in the shape like butter-fly in the comparison with other part of the beam (for the applied point load 500N).

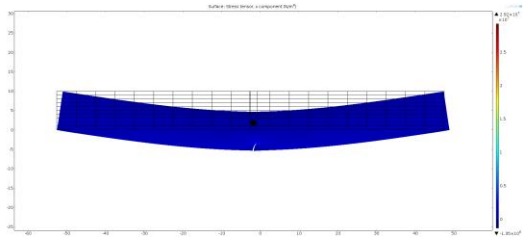

Figure 4:Normal stress distribution in X-direction

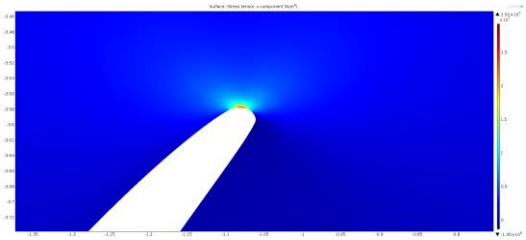

Figure 5: Normal stress distribution in X-direction around the crack tip.

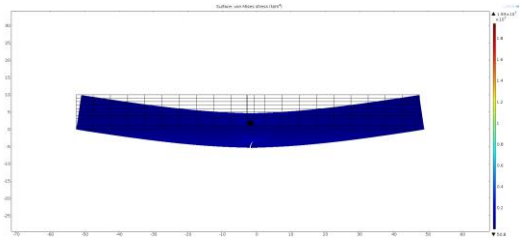

Figure 6: Von-Mises stress distribution for three point bend specimen

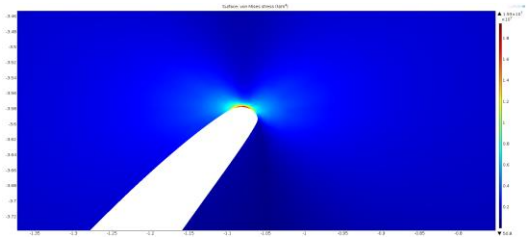

Figure 7: Von-Mises stress distribution around the crack tip for three point bend specimen

Figure 6 represents the variation Von-Mises stress field for the whole beam, which reflect the very high stress concentration near the crack tip with respect to other regions. Dumbbell shaped stress concentration has been seen from COMSOL post processing result analysis around the crack tip as shown in Figure 7.

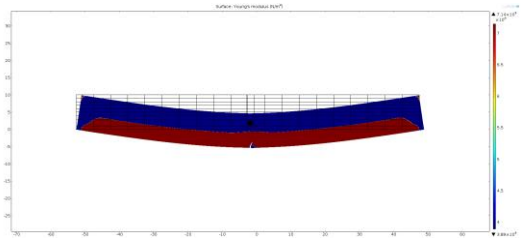

Figure 8: Young's Modulus plot for the three point end specimen

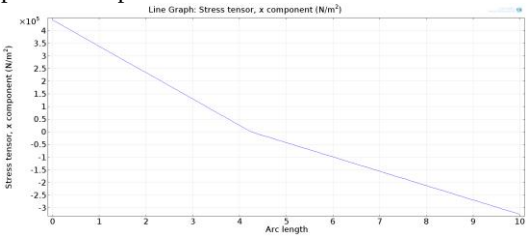

Figure 9: Young's Modulus plot for a cross-section at quarter of the beam and are showing the shift of neutral surface.

The region of compressive and tensile zone is clearly visible by young' modulus of elasticity plot as shown in Figure 8. The shifting of the neutral axis has been evaluated by the linear nodal stress distribution in the vertical linear nodes. In the Figure 9, normal stress in x-direction has been plotted against the vertical nodes by one dimensional line graph at the position of quarter length of the beam from the left end. After the analysis of this graph, the shifting of neutral axis is to be found 0.737 mm downward from middle axis for total height of the beam (10mm). That means 7.35 % of shift is reported for nuclear grade graphite (grade 2020). That relatively reduce the tensile region which take the major role in the flexural failure.

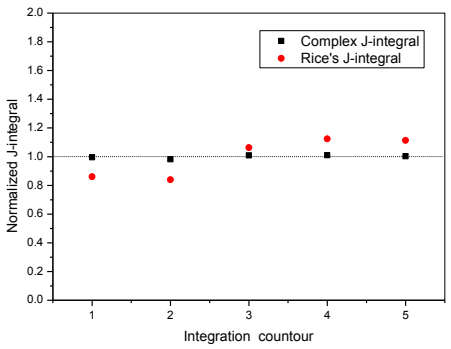

Figure 10. Comaparision of normalized complex *J*-integral vs Rice's J-integral (for E_T/E_C ratio =1.83) at all five contours.

The complex integral $\hat{J}_F$ is very popular integral for characterizing circular arc curve crack in opening mode. But never used in the flexural loading and bimodular stress field condition. The Author's first objective to check path independence of the integral for the unimodular stress field and flexural loading condition. The complex integral $\hat{J}_F$ is found to be path independent, as give us the motivation to check the path independence with the bimodular stress field. And finally, for the bimodular stress field for the nuclear grade graphite (grade 2020) material [37], the complex integral $\hat{J}_F$ is found to be path independent and the value of normalized complex *J*-integral $\hat{J}_F$ (value is normalized by the average value of the five contour value) plotted against the integration contours in the Figure 10. The comparison of complex *J*-integral $\hat{J}_F$ with Rice's *J*-integral [19] has been done. The path independency is lost in the Rice's *J*-integral whereas $\hat{J}_F$ become the independent of its path.

5. Conclusions

The complex integral $\hat{J}_F$, has been found to be path independent computationally for both unimodular and bimodular materials. The degree of path independency for complex J-integral in the comparison of Rice's J-integral [2] is found to very good. The E_T/E_C ratio influences the value of the complex *J*-integral $\hat{J}_F$ significantly as observed by the simulation of nuclear grade graphite grade (2020). Therefore, it is concluded that the effect of the bi-modularity on the computation of complex *J*-integral values cannot be neglected.

6. References

1. Saint-Venant B., "Notes to Navier's Resume des lecons dela resistance des corps solids," 3rd Ed., Paris, 175 (1864).
2. Timoshenko S., "Strength of materials, Part2." Advanced Theory and Problems, 2nd Ed., Van Nostrand, Princeton, N.J., 362–369 (1941).
3. Marin J., "Mechanical behavior of engineering materials," Prentice- Hall, Englewood Cliffs, N.J., 86–88 (1962).
4. Ambartsumyan S.A. "The axisymmetric problem of circular cylindrical shell made of materials with different stiffness in tension and compression." Izvestia Akademiya Nauk SSSR. Meckanika,. (4), 77-85; English Translation (1967), NTIS Report FTD-HT-23-1055-67, Nat. Tech. Info. Service, Springfield, Va (1965),.
5. Ambartsumyan S.A., "Equations of the plane problem of the multimodulus theory of elasticity," Izvestiya Akademii Nauk Armanskoi SSR, Mekhanika, 19(2), 3-19. Translation available from the Aerospace Corp., El Segundo, Calif, as LRG-67-T-14 (1966).
6. Ambartsumyan, S.A., "Basic equations and relations in the theory of elasticity of anisotropic bodies with different moduli in tension and

compression." Inzhenemyi Zhurnal, Mekhanika Tverdogo Tela, 3, 51-61. Translation available from the Aerospace Corp., El Segundo, Calif, as LRG-70-T-1(1969).
7. Bert, C.W. "Models for fibrous composites with different properties in tension and compression," Eng. Mat. and Tech. Trans., ASME, 99H, Oct., 344- 349(1977),.
8. Bert, C.W., "Recent advances in mathematical modeling of the mechanics of bimodulus, fiber-reinforced materials," Proc. 15th Annual Meeting, Society of Eng. Science, Gainesville, Fla., Dec, 101-106, (1978).
9. Green, A.E., and Mkrtichian, J.Z., "Elastic solids with different moduli in tension and compression," J. Elasticity, 7(4), 369-386, (1977).
10. Isabekian, N.G., Khachatryan, A.A., "On the multimodulus theory of elasticity of anisotropic bodies in plane stress state," Ivestiya Akademii Nauk Armianskoi SSR, Mekhanika, 22(5), 25-34. Translation available from R. M. Jones, (1969).
11. Jones, R.M., "Buckling of stiffened multilayered circular cylindrical shells with different orthotropic moduli in tension and compression," AIAA Journal, 9(5), 917-923, (1971).
12. Jones, R.M., "Stress strain relations for materials with different moduli in tension and compression," AIAA Journal, 15(1), 16-23, (1977).
13. Iwase T., Hirashima K., "High-accuracy analysis of beams of bimodulus materials," Journal of Engineering Mechanics, 126, 149-156, (2000).
14. Tran, A.D., Bert, C.W., "Bending of thick beams of bimodulus materials." Computers & Structures 15(6) , 627-642 (1982).
15. Gyekenyesi, J.P., "SCARE: A Postprocessor Program to iSC/NASTRAN for Reliability Analysis of Structural Ceramic Components". 108, 540-546, (1986).

16. Khan, D., Bhushan, A., Panda, S. K., Biswas, K. "Assessment of structural integrity under dynamic loading using path-independent integral $\hat{J}_F$." Mechanics Based Design of Structures and Machines, 41, 434–451, (2013).
17. Eshelby, J. D. "The Continuum Theory of Lattice Defects." Solid State Phsics 3. New York: Academic Press (1956).
18. Cherepanov, G. P. "Crack propagation in continuous media." Appl. Math. Mech. 31, 467–488 (1967).
19. Rice, J.R., "A path independent integral and the approximate analysis of strain concentration by notches and cracks." Trans. ASME, J. Appl. Mech., 35, 379-386, (1968).

20 Sih G.C., "On the Singular Character of Thermal Stresses Near a Crack Tip" Journal of Applied Mechanics, Transactions of the ASME,29 587-589(1962).
21. Kishimoto, K., Aoki, S., Sakata, M., "On the path independent integral $\hat{J}$". Engineering Fracture Mechanics, 13,841-850, (1980)
22. Nishioka, T., "On the dynamic J integral in dynamic fracture mechanics." In: Cherepanov, G. P., ed. FRACTURE: A Tropical Encyclopedia of Current Knowledge (Dedicated to A. A. Griffith). Melbourne: Krieger Publishing Company, pp. 575–617, (1998).
23. Kuntiyawichai, K., Burdekin, F.M., "Engineering assessment of cracked structures subjected to dynamic loads using fracture mechanics assessment." Engg. Fract. Mech. 70, 1991–2014, (2003).
24. Zaho, W., Burdekin, F.M., "Dynamic structural integrity assessment for offshore structures." J. Offsh. Mech. Arct. Engg. ASME. 126,358–363, (2004).
25. Saribay, M., "Three-dimensional elastic-plastic dynamic fracture analysis for stationary cracks under enriched elements Ph.D". Thesis, Lehigh University, (2009).
26. Cotterell, B., Rice, J.R. "Slightly curved or kinked cracks." Int. J. Fract. 16, 155–169, (1980).
27. Lorentzon, M., Eriksson, K. "A path independent integral for the crack extension force of the circular arc crack." Engg. Fract. Mech. 66, 423–439, (2000).
28. Khan, D., Biswas, K., "Circular arc crack under dynamic load: a generalized approach for energy release rate." Int. J. Fract. 141, 27–35, (2006).
29. Khan, D., Biswas, K., "A new conservation integral for circular arc crack under multiple loads." Engg. Fract. Mech. 74, 2375–2394 (2007).
30. Khan, D., Biswas, K., On the evaluation of path independent integral for circular arc crack.

Mechanics Based Design of Structures and Machines, 38, 300–327, (2010).
31. Khan, D., Bhushan, A., Panda, S. K., Biswas, K., "Elastic–plastic dynamic fracture analysis for stationary curved cracks". Finite Elements in Analysis and Design, 73, 55–64, (2013).
32. Choi M.J., Cho, S., "Isogeometric shape design sensitivity analysis of stress intensity factors for curved crack problems." Comput. Methods Appl. Mech. Engrg. 279, 469–496, (2014).
33. Bremberg, D., Faleskog, J., "A numerical procedure for interaction integrals developed for curved cracks of general shape in 3-D." International Journal of Solids and Structures, 62, 144–157, (2015).
34. El-Tahan W.W., Staab G.H., Advani S.H., Lee J.K. " Structural analysis of bimodular materials," Journal of Engineering Mechanics, 115(5), 963–981, (1989).
35. Bhushan, A., Khan, D., Panda, S.K., Chattopadhyay, K., "On the Analysis of J-integral for Nuclear Grade Graphite Specimen" Proceedings of International Conference on Theoretical, Applied, Computational and Experimental Mechanics, December 29-31, IIT Kharagpur, ICTACEM-2014/159, (2014).
36. Bhushan, A., Khan, D., Panda, S.K., Chattopadhyay, K., "Finite Element Evaluation of J-integral in 3D for Nuclear Grade Graphite Using COMSOL-Multiphysics." Proceedings of the COMSOL Conference in Pune (2015).
37. General Atomics "Graphite design handbook", , DOE-HTGR-88111, (1988).
38. COMSOL Multiphysics, version 4.4.

7. Acknowledgements

The authors wish to gratefully acknowledge the financial support for this research provided by BRNS under Grant No. 2011/36/62-BRNS with Indian Institute of Technology (Banaras Hindu University).